Search for Differences in Oscillation Parameters for Atmospheric Neutrinos and Antineutrinos at Super-Kamiokande

K. Abe,[1,3] Y. Hayato,[1,3] T. Iida,[1] M. Ikeda,[1] K. Iyogi,[1] J. Kameda,[1,3] Y. Koshio,[1,3] Y. Kozuma,[1] M. Miura,[1,3]
S. Moriyama,[1,3] M. Nakahata,[1,3] S. Nakayama,[1,3] Y. Obayashi,[1,3] H. Sekiya,[1,3] M. Shiozawa,[1,3] Y. Suzuki,[1,3]
A. Takeda,[1,3] Y. Takenaga,[1] Y. Takeuchi,[1,3,*] K. Ueno,[1] K. Ueshima,[1] H. Watanabe,[1] S. Yamada,[1] T. Yokozawa,[1]
C. Ishihara,[2] H. Kaji,[2] K.P. Lee,[2] T. Kajita,[2,3] K. Kaneyuki,[2,3,†] T. McLachlan,[2] K. Okumura,[2] Y. Shimizu,[2]
N. Tanimoto,[2] K. Martens,[3] M.R. Vagins,[3,6] L. Labarga,[31] L.M. Magro,[31] F. Dufour,[4] E. Kearns,[4,3] M. Litos,[4]
J.L. Raaf,[4] J.L. Stone,[4,3] L.R. Sulak,[4] M. Goldhaber,[5,†] K. Bays,[6] W.R. Kropp,[6] S. Mine,[6] C. Regis,[6] M.B. Smy,[6,3]
H.W. Sobel,[6,3] K.S. Ganezer,[7] J. Hill,[7] W.E. Keig,[7] J.S. Jang,[8] J.Y. Kim,[8] I.T. Lim,[8] J.B. Albert,[9] K. Scholberg,[9,3]
C.W. Walter,[9,3] R. Wendell,[9] T.M. Wongjirad,[9] S. Tasaka,[10] J.G. Learned,[11] S. Matsuno,[11] T. Hasegawa,[13]
T. Ishida,[13] T. Ishii,[13] T. Kobayashi,[13] T. Nakadaira,[13] K. Nakamura,[13,3] K. Nishikawa,[13] H. Nishino,[13]
Y. Oyama,[13] K. Sakashita,[13] T. Sekiguchi,[13] T. Tsukamoto,[13] A.T. Suzuki,[14] A. Minamino,[15] T. Nakaya,[15,3]
Y. Fukuda,[16] Y. Itow,[32,17] G. Mitsuka,[17] T. Tanaka,[17] C.K. Jung,[18] I. Taylor,[18] C. Yanagisawa,[18] H. Ishino,[20]
A. Kibayashi,[20] S. Mino,[20] T. Mori,[20] M. Sakuda,[20] H. Toyota,[20] Y. Kuno,[21] S.B. Kim,[22] B.S. Yang,[22] T. Ishizuka,[23]
H. Okazawa,[24] Y. Choi,[25] K. Nishijima,[26] M. Koshiba,[27] M. Yokoyama,[27] Y. Totsuka,[27,†] S. Chen,[28] Y. Heng,[28]
Z. Yang,[28] H. Zhang,[28] D. Kielczewska,[29] P. Mijakowski,[29] K. Connolly,[30] M. Dziomba,[30] and R.J. Wilkes[30]

(The Super-Kamiokande Collaboration)

[1]*Kamioka Observatory, Institute for Cosmic Ray Research, University of Tokyo, Kamioka, Gifu 506-1205, Japan*
[2]*Research Center for Cosmic Neutrinos, Institute for Cosmic Ray
Research, University of Tokyo, Kashiwa, Chiba 277-8582, Japan*
[3]*Institute for the Physics and Mathematics of the Universe, University of Tokyo, Kashiwa, Chiba 277-8582, Japan*
[4]*Department of Physics, Boston University, Boston, MA 02215, USA*
[5]*Physics Department, Brookhaven National Laboratory, Upton, NY 11973, USA*
[6]*Department of Physics and Astronomy, University of California, Irvine, Irvine, CA 92697-4575, USA*
[7]*Department of Physics, California State University, Dominguez Hills, Carson, CA 90747, USA*
[8]*Department of Physics, Chonnam National University, Kwangju 500-757, Korea*
[9]*Department of Physics, Duke University, Durham NC 27708, USA*
[10]*Department of Physics, Gifu University, Gifu, Gifu 501-1193, Japan*
[11]*Department of Physics and Astronomy, University of Hawaii, Honolulu, HI 96822, USA*
[12]*Physics Division, Department of Engineering, Kanagawa University, Kanagawa, Yokohama 221-8686, Japan*
[13]*High Energy Accelerator Research Organization (KEK), Tsukuba, Ibaraki 305-0801, Japan*
[14]*Department of Physics, Kobe University, Kobe, Hyogo 657-8501, Japan*
[15]*Department of Physics, Kyoto University, Kyoto, Kyoto 606-8502, Japan*
[16]*Department of Physics, Miyagi University of Education, Sendai, Miyagi 980-0845, Japan*
[17]*Solar Terrestrial Environment Laboratory, Nagoya University, Nagoya, Aichi 464-8602, Japan*
[18]*Department of Physics and Astronomy, State University of New York, Stony Brook, NY 11794-3800, USA*
[19]*Department of Physics, Niigata University, Niigata, Niigata 950-2181, Japan*
[20]*Department of Physics, Okayama University, Okayama, Okayama 700-8530, Japan*
[21]*Department of Physics, Osaka University, Toyonaka, Osaka 560-0043, Japan*
[22]*Department of Physics, Seoul National University, Seoul 151-742, Korea*
[23]*Department of Systems Engineering, Shizuoka University, Hamamatsu, Shizuoka 432-8561, Japan*
[24]*Department of Informatics in Social Welfare, Shizuoka University of Welfare, Yaizu, Shizuoka, 425-8611, Japan*
[25]*Department of Physics, Sungkyunkwan University, Suwon 440-746, Korea*
[26]*Department of Physics, Tokai University, Hiratsuka, Kanagawa 259-1292, Japan*
[27]*The University of Tokyo, Bunkyo, Tokyo 113-0033, Japan*
[28]*Department of Engineering Physics, Tsinghua University, Beijing, 100084, China*
[29]*Institute of Experimental Physics, Warsaw University, 00-681 Warsaw, Poland*
[30]*Department of Physics, University of Washington, Seattle, WA 98195-1560, USA*
[31]*Department of Theoretical Physics, University Autonoma Madrid, 28049 Madrid, Spain*
[32]*Kobayashi-Maskawa Institute for the Origin of Particle and the Universe, Nagoya University, Nagoya, Aichi 464-8602, Japan*
(Dated: October 22, 2018)

We present a search for differences in the oscillations of antineutrinos and neutrinos in the Super-Kamiokande -I, -II, and -III atmospheric neutrino sample. Under a two-flavor disappearance model with separate mixing parameters between neutrinos and antineutrinos, we find no evidence for a difference in oscillation parameters. Best fit antineutrino mixing is found to be at $(\Delta\bar{m}^2, \sin^2 2\bar{\theta}) = (2.0 \times 10^{-3}\text{eV}^2, 1.0)$ and is consistent with the overall Super-K measurement.

arXiv:1109.1621v2 [hep-ex] 25 Oct 2011

As the parameters outlining the standard neutrino oscillation framework become increasingly well known, searches for sub-leading and possibly symmetry-breaking effects become possible. If the value of θ_{13} is non-zero, for instance, it becomes possible to search for CP-violation effects in the neutrino system via differences in the oscillation probabilities of neutrinos and antineutrinos. In this paper we consider the possibility that the survival probability $P(\nu_\mu \to \nu_\mu)$ is governed by a different mass splitting or mixing angle compared to $P(\bar{\nu}_\mu \to \bar{\nu}_\mu)$. This is not considered in most oscillation studies as the mass splitting and mixing angle are expected to be identical for neutrinos and antineutrinos by CPT symmetry. An inequality of these probabilities, in the absence of matter effects, could signal new physics. For atmospheric muon neutrino disappearance, which is predominantly oscillation into tau neutrinos, the matter effect is expected to be small and the mixing parameters for muon neutrino and antineutrino disappearance appearance should be the same. The MINOS experiment, which is sensitive to neutrino oscillations at the atmospheric scale, and which can determine the sign of muons by magnetic bending, has observed antineutrino disappearance [1] at a best-fit value of Δm^2 nearly 50% larger than previous measurements made using neutrinos [2–5]. Though not in the realm of atmospheric mixing, the MiniBooNE experiment has similarly observed a discrepancy between its neutrino [6] and antineutrino [7] data. Therefore, further tests of differences between neutrinos and antineutrinos using atmospheric data are well motivated.

Super-Kamiokande (Super-K, SK), described below, cannot distinguish ν from $\bar{\nu}$ on an event by event basis so potential differences in their oscillations would appear in the atmospheric neutrino sample in a statistical way. Notably, the neutrino and antineutrino cross sections differ by a factor of two to three depending on the neutrino energy. The ratio of the ν and $\bar{\nu}$ atmospheric fluxes is similarly energy dependent [8]. For these reasons, even in the absence of CPT-violating oscillations the relative numbers of each species are expected to differ. Kinematic considerations can also induce differences in the products of neutrinos and antineutrino reactions, enhancing the sample purity of one or the other. For instance, the absorption of π^- on ^{16}O nuclei in water tends to enrich the neutrino component of samples that are sub-divided based on their number of decay electrons. If CPT-violating oscillations are present in the data, the distortion of the zenith angle distribution characteristic of ν_μ disappearance would appear at different energies and path lengths (different oscillation frequencies) between neutrinos and antineutrinos. Since Super-K can only observe the total distribution, a potential signal would appear as a distortion consistent with the com-

position of separately oscillated spectra. In this context, antineutrinos, which have the smaller cross section, are expected to provide a weaker oscillation constraint than neutrinos.

In this Letter we consider *ad-hoc* CPT-violating oscillations by testing separate two-neutrino disappearance models for neutrinos and antineutrinos:

$$
\begin{aligned}
P(\nu_\mu \to \nu_\mu) &= 1 - \sin^2 2\theta \sin\left(\frac{\Delta m^2 L}{4E}\right) \\
P(\bar{\nu}_\mu \to \bar{\nu}_\mu) &= 1 - \sin^2 2\bar{\theta} \sin\left(\frac{\Delta \bar{m}^2 L}{4E}\right),
\end{aligned} \tag{1}
$$

where L is the neutrino path-length and E is the neutrino energy. In the presence of matter, additional neutrino-electron scattering induces a CPT-violating-like difference between the neutrino and antineutrino survival probabilities [9, 10], particularly when θ_{13} is non-zero. Recent data suggest [11–13] that θ_{13} is small and therefore matter-induced corrections to Eqn. 1 are expected to be sub-dominant. Changes to the fit results induced by a three-flavor treatment are briefly considered below. Although the presence of both matter and solar mixing terms is expected to drive $\nu_\mu \to \nu_e$ transitions below about 1 GeV even if $\theta_{13} = 0$, the oscillation frequency in this domain is high enough that the effects are averaged out by the detector resolution. Since the dominant atmospheric disappearance effect is seen at higher energies, a two-neutrino scheme is the focus of this study.

Super-Kamiokande is a water Cherenkov detector located in Japan's Gifu prefecture and situated at a depth of 2700 meters water equivalent. It is comprised of two concentric, optically separated cylinders: an inner detector (ID) viewing a 22.5 kton fiducial volume and an outer detector (OD) used primarily as a veto. During the first run of the detector, SK-I, the walls of the ID were lined with 11,146 inward-facing 20-inch photomultiplier tubes (PMTs). The two subsequent run periods, SK-II and SK-III, had 5,182 and 11,129 ID PMTs, respectively and the PMTs have been encased in fiber-reinforced plastic shells. The OD has been instrumented with 1,885 outward-facing 8-inch PMTs throughout. More details on the detector and its calibration may be found in [14].

The atmospheric neutrino data are divided into three categories. Fully contained (FC) events deposit all of their light in the ID, partially contained (PC) events additionally have an exiting particle that deposits energy in the OD, and upward-going muon (Up-μ) events are produced by neutrino interactions in the rock beneath the detector. Up-μ events are required to have a minimum pathlength of seven meters and are classified as stopping or through-going. Through-going Up-μ events are further sub-divided into "showering" and "non-showering" based on [15].
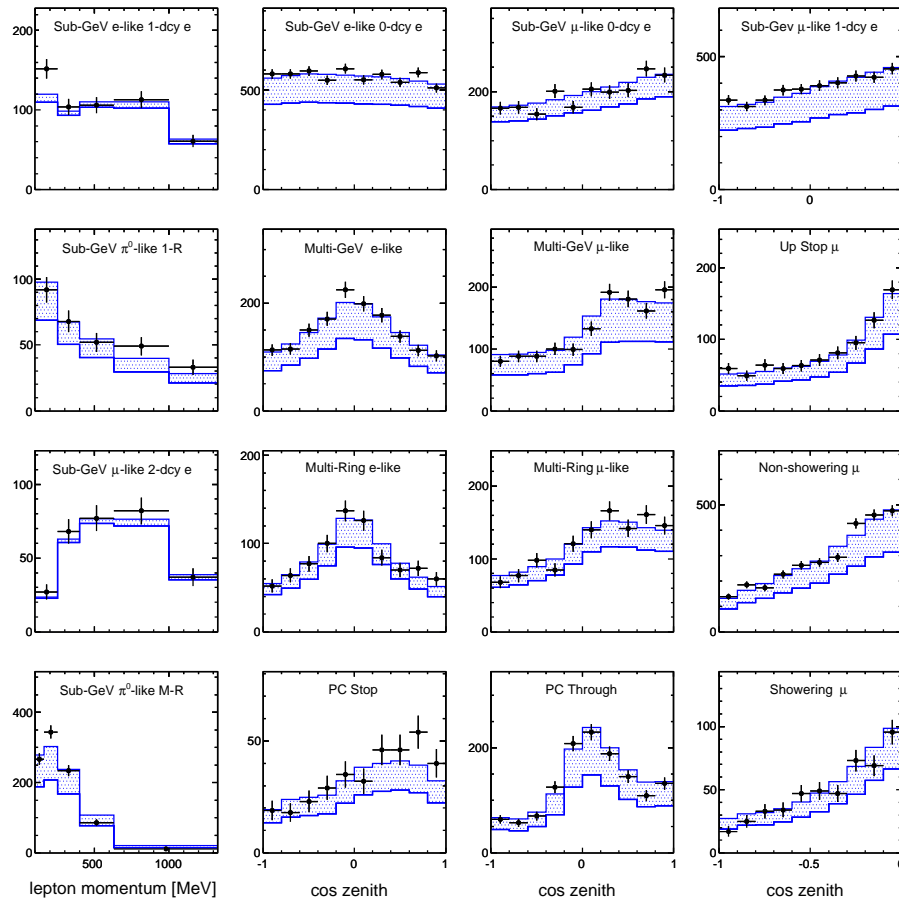
FIG. 1: SK-I+II+III lepton momentum (first column) and zenith angle distributions of the event samples used in the analysis. Black dots represent the data with statistical errors, the histogram is the oscillated MC expectation at the best fit point with the shaded region showing the antineutrino composition.

The present analysis uses data accumulated during the first three SK run periods. SK-I (1996 to 2001) FC and PC events correspond to 1489 live-days with 1646 days of Up-μ livetime. SK-II (2002 to 2005) had 799 FC/PC and 828 live-days of Up-μ events. The FC and PC livetimes during SK-III (2005-2007) were 518 days and that for Up-μ was 636 days.

During the analysis, FC and PC events are further divided. Fully contained events are separated into sub-GeV (E_{vis} < 1.33 GeV) and multi-GeV (E_{vis} > 1.33 GeV). These samples are then separated based on their number of reconstructed Cherenkov rings into single- and multi-ring topologies. Pattern-identification of single-ring events is used to separate them into e-like and μ-like

categories. This technique is applied to the multi-ring sample using the most energetic Cherenkov ring. The sub-GeV single-ring e-like and μ-like samples are also divided based upon their number of decay-electrons. A π^0-like sample is also extracted from the single-ring e-like events [12]. Partially contained events are separated into "OD stopping" and "OD through-going" categories based on the amount of Cherenkov light observed in the OD at the exit point.

Since the physical configuration of the detector and its reconstruction performance varies among the SK run periods, separate 500 year MC samples are used for each. A "pulled" χ^2 [16] based on a Poisson probability distribution is used to compare the data against the MC:

$$\chi^2 \;=\; 2\sum_n \left(\sum_i E_n^{SKi}(1 + \sum_j f_n^j \epsilon_j) - \sum_i \mathcal{O}_n^{SKi} + \sum_i \mathcal{O}_n^{SKi} \ln \frac{\sum_i \mathcal{O}_n^{SKi}}{\sum_i E_n^{SKi}(1 + \sum_j f_n^j \epsilon_j)} \right) + \sum_k \left(\frac{\epsilon_k}{\sigma_k} \right)^2. \quad (2)$$

In this equation n indexes the data bins, E_n^{SKi} is the MC expectation for SK-i, and $\mathcal{O}_n^{SKi}$ is the number of observed events in the nth bin during SK-i. The effect of the ith systematic error is introduced via the error parameter ϵ_i and f_n^i, where the latter is the fractional change in the MC expectation of bin n introduced by a 1-sigma shift in its systematic error, σ_i. The data and MC are divided into 420 bins for each of the SK run periods when computing these systematic errors, but are later merged as above to ensure the stability of the fit function against sparsely populated bins. In total, 420 bins are used to compute the value of χ^2.

Equation (2) is minimized with respect to the ϵ_i according to $\frac{\partial \chi^2}{\partial \epsilon_i} = 0$, yielding a set of linear equations in ϵ_i that are solved iteratively [16]. Following this procedure a χ^2 value is computed for each point in the oscillation parameter space. The global minimum χ^2 is defined as the analysis' best fit point.

Parameter	Best Fit	90% C.L.	Three-Flavor
$\Delta m^2(\text{eV}^2)$	2.1×10^{-3}	$[\,1.7\,,\,3.0\,] \times 10^{-3}$	$[\,1.7\,,\,3.3\,] \times 10^{-3}$
$\Delta \bar{m}^2(\text{eV}^2)$	2.0×10^{-3}	$[\,1.3\,,\,4.0\,] \times 10^{-3}$	$[\,1.2\,,\,4.0\,] \times 10^{-3}$
$\sin^2 2\theta$	1.0	$[\,0.93,\,1.0\,]$	$[\,0.93,\,1.0\,]$
$\sin^2 2\bar{\theta}$	1.0	$[\,0.83,\,1.0\,]$	$[\,0.78,\,1.0\,]$

TABLE I: Best fit information for the four parameter fit to the SK-I+II+III data. The 90% C.L. column represents bounds taken from single-parameter $\Delta\chi^2$ distributions in which the remaining three parameters have been minimized over. The third column shows the 90% C.L. allowed region when the effects of θ_{13} and δ_{cp} are considered in the fit (see text).

The 120 sources of systematic uncertainty considered in this analysis are separated into two classes: those that are common throughout the SK run periods and those that are dependent upon a particular detector geometry. Common systematic errors stem from uncertainties in the neutrino interaction cross sections, nuclear effects, and the atmospheric neutrino flux. Independent systematic errors are related to detector performance and include uncertainties in the event reconstruction and reduction. A complete list of the systematic errors used here is presented in [12].

Antineutrino oscillations are considered independently of neutrino oscillations over a four-dimensional oscillation space with two parameters for each: ($\Delta\bar{m}^2$, $\sin^2 2\bar{\theta}$) and (Δm^2, $\sin^2 2\theta$). All parameters are varied simultaneously on a grid of 50×35 points in the antineutrino plane and 20×10 points in the neutrino plane. The neutrino(antineutrino) parameter space is taken over $1.0(0.7) \times 10^{-3} \leq \Delta m^2 \leq 5.0(8.0) \times 10^{-3}\text{eV}^2$ and $0.85(0.65) \leq \sin^2 2\theta \leq 1.0(1.0)$, comprising an area encompassing the current allowed values of these parameters [5, 12]. Minimizing the χ^2 function in Eqn. 2
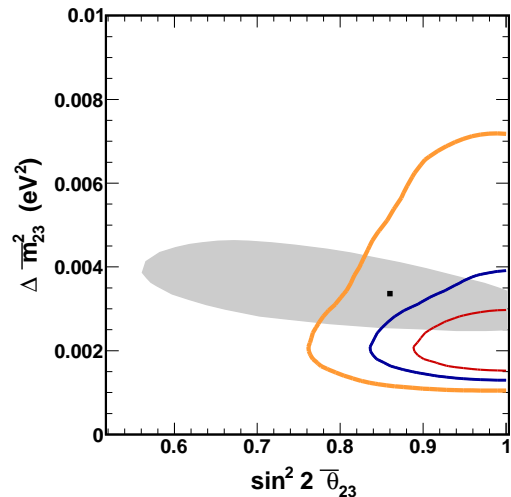

FIG. 2: Allowed regions for the antineutrino mixing parameters for the SK-I+II+III data set. The 68%, 90%, and 99% allowed region appear in thin, medium, and thick lines respectively. The shaded region shows the 90% C.L. allowed region for antinuetrino disappearance in an antineutrino beam from MINOS [1]. A solid point denotes the location of the best fit from that analysis.

over this parameter space, the best fit is found with $\chi^2 = 468.4$ for 416 degrees of freedom. Table I summarizes the fit information. Since the oscillations of atmospheric neutrinos are sensitive to the effects of θ_{13} and δ_{cp}, an additional analysis has been performed assuming distinct three-flavor mixing between neutrinos and antineutrinos. Though this model has no strong theoretical motivation, the potential impact of a three-flavor framework on the SK allowed regions is provided in the table for reference. In both fits no difference between antineutrino and neutrino mixing is found in the data.

The combined data overlaid with the MC expectation at the best fit point are shown in Fig. 1. Antineutrinos have been oscillated independently of neutrinos in the expectation and are shown as the shaded portion of the histogram. Figure 2 shows the allowed regions at several C.L. in the antineutrino plane. The neutrino parameters have been minimized over and the contours have been drawn for a standard $\Delta\chi^2$ distribution with two degrees of freedom. The 90% C.L. regions from the antineutrino and neutrino parameters overlaid with the allowed region from the standard two-flavor analysis, where the mixing parameters are required to be identical for neutrinos and antineutrinos, appear in Fig. 3. The best fit point of the standard analysis, (Δm^2, $\sin^2 2\theta$) = ($2.1 \times 10^{-3}\text{eV}^2$, 1.0), is consistent with the best fit from the antineutrino separated analysis.

At each point in the plane of Fig. 2 the best fit to the data may lie at a point in the neutrino parameters that does not correspond to equal neutrino and antineu-
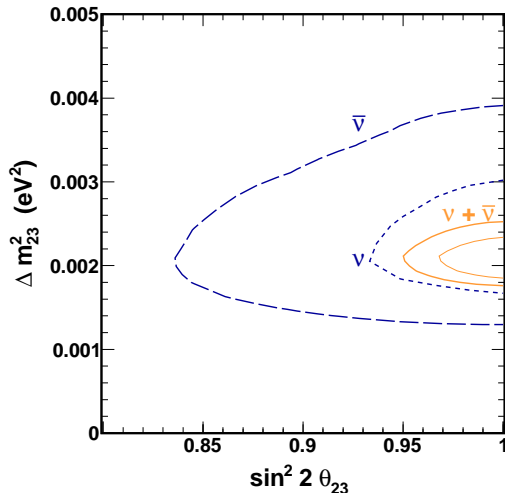
FIG. 3: Allowed regions for atmospheric mixing parameters from the SK-I+II+III data set. The 68% and 90% C.L. interval from the standard two-flavor analysis with equal neutrino and antineutrino oscillations shown by thin and thick solid lines, respectively. The 90% C.L. contour for neutrinos (least expansive) and antineutrinos (most expansive) from the current analysis are dashed.
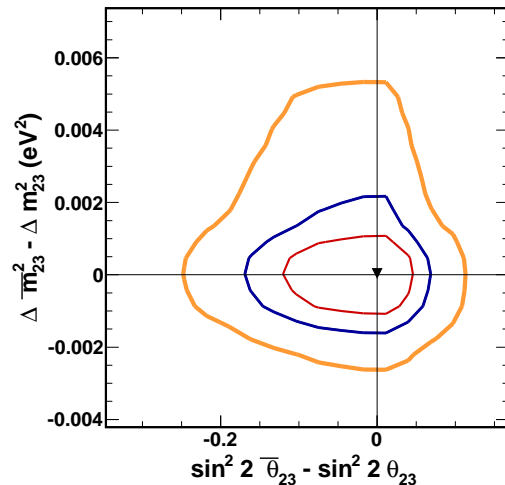

FIG. 4: Allowed differences between neutrino and antineutrino oscillation parameters for the SK-I+II+III data set. The 68%, 90%, and 99% allowed region appear in thin, medium, and thick lines, respectively. A black triangle shows the location of the best fit point from this analysis.

trino mixing. To illustrate the difference between neutrino and antineutrino oscillations permitted by the data, Fig. 4 shows the allowed regions as a function of the difference of the antineutrino and neutrino mixing angles, $\sin^2 2\bar\theta - \sin^2 2\theta$, and mass squared splittings, $\Delta\bar m^2 - \Delta m^2$. Contours have been drawn as in Fig. 2 and a black triangle near the origin represents the position of the best fit.

In conclusion, a search for evidence of differing neutrino and antineutrino oscillation parameters in the SK-I+II+III atmospheric data sample has been carried out. The atmospheric mixing parameters for antineutrino oscillations are consistent with those for neutrino oscillation. The results agree with the standard SK atmospheric oscillation analysis, which have also been presented. The SK antineutrino oscillation best fit is consistent with the parameters found by MINOS using a predominantly muon neutrino beam.

We gratefully acknowledge the cooperation of the Kamioka Mining and Smelting Company. The Super-Kamiokande experiment has been built and operated from funding by the Japanese Ministry of Education, Culture, Sports, Science and Technology, the United States Department of Energy, and the U.S. National Science Foundation. Some of us have been supported by funds from the Korean Research Foundation (BK21), and the Korea Research Foundation Grants (MOEHRD, Basic Research Promotion Fund), (KRF-2008-521-c00072). Some of us have been supported by the State Committee for Scientific Research in Poland

---

* Present address Department of Physics, Kobe University, Kobe, Hyogo 657-8501, Japan
† Deceased.
[1] P. Adamson et al. (MINOS), Phys. Rev. Lett. **107**, 021801 (2011), 1104.0344.
[2] J. Hosaka et al. (Super-Kamiokande), Phys. Rev. **D74**, 032002 (2006), hep-ex/0604011.
[3] Y. Ashie et al. (Super-Kamiokande), Phys. Rev. **D71**, 112005 (2005), hep-ex/0501064.
[4] M. H. Ahn et al. (K2K), Phys. Rev. **D74**, 072003 (2006), hep-ex/0606032.
[5] P. Adamson et al. (MINOS), Phys. Rev. Lett. **101**, 131802 (2008), 0806.2237.
[6] A. A. Aguilar-Arevalo et al. (MiniBooNE), Phys. Rev. Lett. **98**, 231801 (2007), 0704.1500.
[7] A. Aguilar-Arevalo et al. (MiniBooNE), Phys.Rev.Lett. **105**, 181801 (2010), 1007.1150.
[8] M. Honda, T. Kajita, K. Kasahara, S. Midorikawa, and T. Sanuki, Phys. Rev. **D75**, 043006 (2007), astro-ph/0611418.
[9] S. P. Mikheev and A. Y. Smirnov, Sov. J. Nucl. Phys. **42**, 913 (1985).
[10] L. Wolfenstein, Phys. Rev. **D17**, 2369 (1978).
[11] M. Apollonio et al. (Chooz), Eur. Phys. J. **C27**, 331 (2003), hep-ex/0301017.
[12] R. Wendell et al. (Super-Kamiokande), Phys. Rev. **D81**, 092004 (2010), arXiv:1002.3471.
[13] K. Abe et al. (T2K), Phys.Rev.Lett. **107**, 041801 (2011),

1106.2822.

[14] Y. Fukuda et al. (Super-Kamiokande), Nucl. Instrum. Meth. **A501**, 418 (2003).

[15] S. Desai et al. (Super-Kamiokande), Astropart. Phys. **29**, 42 (2008), 0711.0053.

[16] G. L. Fogli, E. Lisi, A. Marrone, D. Montanino, and A. Palazzo, Phys. Rev. **D66**, 053010 (2002), hep-ph/0206162.